

Optical fiber reliability implications of uncertainty in the fatigue crack growth model

G. M. Bubel

AT&T Bell Laboratories
Crawfords Corner Road
Holmdel, New Jersey 07733

M. J. Matthewson

Rutgers University
Fiber Optic Materials Research Program
Ceramic Science and Engineering
P.O. Box 909
Piscataway, New Jersey 08855

Abstract. Prediction of long-term static fatigue for optical fibers under stress requires a model to relate short-term accelerated test results to long-term behavior. The dependence of crack growth on stress intensity is the most fundamental model for this reliability prediction process. Statistical uncertainty for fatigue testing is shown to be significant, but typically smaller than the model uncertainty, which has been neglected in the literature. More research is needed to determine the most appropriate model. It is shown that the differences in allowed stress predictions between models become quite large at long times, especially for fiber of the same strength as that used in the fatigue test. Data-independent conversions of allowed stress from the common power model to other models provide an assessment of the difference between models for various situations. In many applications, the differences are in the range of typical safety factors. However, since model differences are quite large in other applications, universal use of the optimistic power law model is not appropriate, given the limited understanding of fatigue in optical fibers.

Subject terms: optical fiber reliability; fiber fatigue; crack growth models.

Optical Engineering 30(6), 737-745 (June 1991).

CONTENTS

1. Introduction
2. Flaw growth mechanisms
3. Statistical and model uncertainty in static fatigue predictions
4. Dispersion in failure time
5. Proof testing
6. Summary and discussion
7. Acknowledgments
8. References

1. INTRODUCTION

The practical strength of glass, and of optical fibers in particular, is controlled by flaws, usually on the surface. It is well established, furthermore, that such flaws can grow in time so that an initially intact silica optical fiber may undergo delayed fracture from the combined influence of low stress levels and the chemical environment. When optical fibers are deployed in high-reliability applications, a model of the crack growth kinetics is used to predict, from accelerated laboratory experiments, the conditions under which delayed failure will occur.

The current practice of modeling crack growth is usually based on an assumed power law dependence of crack velocity on stress intensity. Integration of this function leads to an expression relating failure time to strength and applied stress. This relationship depends on empirically determined fatigue parameters. While statistical uncertainty in these derived fatigue parameters has been discussed,^{1,2} the uncertainty in the crack ve-

locity model itself has usually been overlooked. Some analysis has been made of the differences between possible crack velocity models for bulk ceramics.³⁻⁵ In these studies, fatigue data are fit to different models, and the conclusion was that several models provide about the same degree of fit, but quite different extrapolations of time to failure. However, time to failure is not a useful comparison of models, since allowed stress for a given failure time is the more commonly required information. Also lacking are a comparison of model differences with statistical uncertainty, and comparisons between models in their prediction of low strength reliability and proof test effectiveness. In this paper, these differences between the models are quantified for fatigue projections from real data. In addition, translations of predictions from the common power law to other models are developed in a data-independent formulation.

2. FLAW GROWTH MECHANISMS

The slow growth of a crack in silica arises from a stress-enhanced corrosion of the SiO₂ structure. Some research has addressed the chemical dynamics of this process.^{6,7} These studies explain the strong effect of water in promoting crack growth and provide some independent assessment of the observed dependence of crack growth on stress. Nonwater chemical environments can also contribute to stress corrosion of silica. Michalske and Bunker⁸ suggest a steric effect to explain some observed differences between environments. Yuce et al.⁹ studied the effect on actual fibers of various common chemicals. In practice, avoiding reactive species, especially water, is difficult. Thus, the typical reliability problem is to predict the allowed long-term fiber stress from stress accelerated testing in a similar environment. Crack growth chemistry and its kinetics are not sufficiently understood to allow extrapolation from one environment to another.

Invited paper OFR-7 received Feb. 20, 1991; revised manuscript received March 1, 1991; accepted for publication March 1, 1991.
© 1991 Society of Photo-Optical Instrumentation Engineers.

Fatigue testing performed in high-temperature water immersion sometimes shows a stress-independent effect, the "transition" or "knee" in the stress versus time to failure relation.^{10,11} This effect correlates strongly with strength reduction at zero stress in the same environment. The mechanism for the behavior is not known; it may be a dissolution-like mechanism that becomes operative at long times.¹² Studies have shown that some coatings can prevent, or at least delay, this effect.^{11,13} The effect is also absent from fatigue data in less severe environments. These data along with an empirically determined temperature dependence of the "transition" onset¹⁴ suggest that the effect may not be important in many practical environments. Further understanding of the mechanism is needed, however, to test this tentative conclusion. The analysis in this paper deals only with the stress-enhanced flaw growth reaction, which is clearly operative in nearly all practical environments (for nonhermetic fiber).

The models that have been proposed for making static fatigue reliability predictions for silica fiber are all based on crack growth kinetic models that assume that the strength of the fiber depends on the presence of well-defined sharp cracks whose severities are uniquely defined by one parameter; their length c . However, the presence of such cracks in high-strength silica has never been demonstrated. Indeed, strong evidence exists that pristine fiber is essentially flaw free since the liquid nitrogen (i.e., inert) strength of pristine fiber is single valued and close to the theoretical strength of the material.¹² Reliability predictions for pristine fiber, therefore, must be considered empirical extrapolations not based on a well-defined or understood physical model.

The strength of multikilometer lengths of fiber is well known to be significantly lower than the pristine strength, so reliability predictions must extrapolate on initial strength as well as applied stress. However, the defects leading to low-strength failure are often identified with extrinsic defects such as particles that become adhered to or abrade the fiber surface during drawing or handling. Such defects are usually associated with residual thermal or plastic deformation induced stresses. Therefore, weaker fiber also may not contain well-defined cracks, and, even if cracks are present, their growth kinetics will be significantly perturbed by the residual stresses. Clearly then, extrapolation from pristine fatigue to weaker fiber fatigue is questionable since the nature of the defects is changing. This difficulty is compounded by the lack of any systematic empirical studies of fiber fatigue as a function of the initial fiber strength, though some limited data have been published.¹⁵ Low-load Vickers indentations have been proposed as a model for weak fibers since the plastic deformation produced by the indents leaves a residual stress field similar to that around handling damage sites and adhering particles.¹⁶ Dabbs and Lawn¹⁶ found that microindentations made at sufficiently low indent loads to avoid crack formation had an apparent fatigue parameter n of about 20, similar to the value for high-strength fiber. Later work extended the post-indent strengths to those more typical of fiber proof test levels and found a similar result.¹⁷ Therefore, there might be enough similarity between pristine and weaker fiber to give some confidence in the extrapolations. However, note that the cited n values reflect the measured fatigue dependence on applied stress, not the dependence on inert strength.

Several difficulties with applying crack growth models to high-strength fiber fatigue have been discussed. However, from an engineering viewpoint, reliability estimates have to be made whatever the state of academic understanding of the phenom-

non. In the absence of any other model for fatigue, crack growth kinetics must be used, but their predictions should naturally be considered with conservatism if not skepticism.

3. STATISTICAL AND MODEL UNCERTAINTY IN STATIC FATIGUE PREDICTIONS

Depending on the level of sophistication used, it can be a straightforward task to predict the fiber lifetime from accelerated testing data. However, there is little value in such an estimate without some knowledge of the confidence level. Calculating the confidence interval is considerably more difficult than calculating the expected lifetime, and, perhaps because of this, rigorous analyses of confidences are usually not attempted in the literature. Some published studies have considered statistical uncertainty, i.e., uncertainty in extrapolation arising from statistical variability in the results of accelerated tests. However, such statistical analyses assume that all the uncertainty is in the parameters that characterize the particular fatigue model used but ignore the uncertainty in the nature of the model itself. As we have seen, we do not have a detailed understanding of the fatigue mechanisms in high-strength silica fiber. Therefore, any reasonable fatigue model could be used, but each different model would provide different results for reliability predictions. In this section, we compare the uncertainty in reliability predictions from both statistical and model sources. The uncertainty due to the model will be examined by considering a range of subcritical crack growth models.

It has now been well established that for ceramic materials containing macroscopic cracks, subcritical crack growth results from chemical attack of strained bonds at the crack tip. The rate of attack, and hence the crack growth velocity, is found to be dependent on the intensity of the stress field around the crack tip as quantified by K_I , the mode I stress intensity factor. The following four relationships between crack velocity and K_I will be considered:

$$\frac{dc}{dt} = A_1 \left(\frac{K_I}{K_{IC}} \right)^{n_1}, \quad \text{model 1 (1)}$$

$$\frac{dc}{dt} = A_2 \exp \left[n_2 \left(\frac{K_I}{K_{IC}} \right) \right], \quad \text{model 2 (2)}$$

$$\frac{dc}{dt} = A_3 \exp \left[n_3 \left(\frac{K_I}{K_{IC}} \right)^2 \right], \quad \text{model 3 (3)}$$

$$\frac{dc}{dt} = A_4 \left(\frac{K_I}{K_{IC}} \right) \exp \left[n_4 \left(\frac{K_I}{K_{IC}} \right) \right], \quad \text{model 4 (4)}$$

where c is the crack length and K_{IC} is the critical stress intensity factor for fast fracture.

Model 1 (Refs. 18, 19) is not based on any physical model for the fatigue, but is empirically found to fit a range of fatigue data well. Model 1 is mathematically the most tractable of the four and, probably for this reason, has been most widely used.

Model 2 (Ref. 20) is based on simple chemical kinetic theory in which the reaction rate is given by an Arrhenius type of behavior and where the stress influences the activation energy through an activation volume. Model 3 (Ref. 21) is based on an atomistic model of crack growth, while model 4 (Ref. 22) is a modification of model 2.

When the effect of temperature is also needed, an Arrhenius model is typically used. Temperature acceleration is useful for reliability testing, but it is limited by the effects of high temperature on polymer fiber coatings. Acceleration by increased humidity provides conservatism, but this effect is not sufficiently understood to allow extrapolation. Therefore, the dependence of crack growth on stress intensity is the most important model from a reliability prediction and design point of view.

Note that model 1 is different from the other models in temperature dependence. The temperature dependence of crack growth is usually considered as Arrhenius and is contained in the A_i ($i = 1$ through 4) prefactors. However, for models 2 to 4, K_I influences the activation energy, and so n_2 , n_3 , and n_4 contain temperature dependence while the prefactors contain Arrhenius dependence on the zero stress activation energy. In contrast, model 1 implies that the activation energy is stress independent, which is unphysical and is contradicted by experiment.²³

K_I is related to the crack length and the applied stress σ by the well-known fracture mechanics relation

$$K_I = Y\sigma\sqrt{c} \quad (5)$$

where Y is a dimensionless factor of order unity dependent on the crack geometry. Equations (1) through (4) can be integrated using Eq. (5) to determine the time to failure t_f of a crack subjected to a constant applied stress σ (Refs. 3 and 5):

$$t_f\sigma^2 = \frac{2K_{IC}^2}{A_1Y^2(n_1 - 2)} \left(\frac{\sigma}{S}\right)^{2-n_1} \quad (6)$$

$$t_f\sigma^2 = \frac{2K_{IC}^2}{A_2n_2Y^2} \exp\left[-n_2\left(\frac{\sigma}{S}\right)\right] \left(\frac{\sigma}{S} + \frac{1}{n_2}\right) \quad (7)$$

$$t_f\sigma^2 = \frac{K_{IC}^2}{A_3n_3Y^2} \exp\left[-n_3\left(\frac{\sigma}{S}\right)^2\right] \quad (8)$$

$$t_f\sigma^2 = \frac{2K_{IC}^2}{A_4n_4Y^2} \exp\left[-n_4\left(\frac{\sigma}{S}\right)\right] \quad (9)$$

for models 1 through 4, respectively, where S is the initial inert strength of the material (inert strength \equiv the strength in the absence of fatigue). The equations are derived using the excellent approximation that the starting crack length (corresponding to an inert strength S) is much less than the crack length at which the crack propagates unstably (corresponding to an inert strength σ).

These equations may be linearized for ease in fitting to experimental t_f versus σ data. The linearized forms are:

$$\ln(t_f) = -m_1 \ln(\sigma) + \alpha_1 \quad (10)$$

$$\ln(t_f\sigma) = -m_2(\sigma) + \alpha'_2 \quad (11a)$$

$$\ln[(t_f\sigma^2)/(\sigma/S + 1/n_2)] = -m_2(\sigma) + \alpha_2 \quad (11b)$$

$$\ln(t_f\sigma^2) = -m_3(\sigma^2) + \alpha_3 \quad (12)$$

$$\ln(t_f\sigma^2) = -m_4(\sigma) + \alpha_4 \quad (13)$$

where

$$m_1 = n_1, \quad m_2 = n_2/S, \quad m_3 = n_3/S^2, \quad m_4 = n_4/S \quad (14)$$

Equation (7) cannot be exactly linearized but note that the term $(1/n_2)$ is small compared to the term σ/S so that a close estimate of n_2 can be obtained by fitting data to Eq. (11a). This estimate of n_2 can then be used to obtain a better estimate from Eq. (11b). After only a couple of iterations using Eq. (11b), the value of n_2 is determined to better than 1 ppm. In fact, the estimates for n_2 determined from Eq. (11a) and estimates based on iteration with Eq. (11b) only differed by a fraction of 1% for the two sets of typical data discussed later, and this difference is more than 10 times smaller than the standard error in the estimates. Therefore a single regression using Eq. (11a) will usually be enough to obtain n_2 .

Figure 1 shows the regression fits for power law fatigue [Eq. (10)] to static fatigue data of Wang and Zupko²⁴ for "SS2" laser drawn fiber tested in tension at 90% relative humidity and 32.6°C. Also shown is the power law fit to data of Brownlow et al.²⁵ for AT&T fiber with D-Lux dual coating tested in two-point bending, 80% relative humidity, and 80°C. The solid lines are the best fit, while the dashed lines represent a 95% confidence interval on the extrapolated behavior. Linear regression gives the best fit and variances on the intercept c and slope m in the equation

$$y = mx + c \quad (15)$$

However, the covariance of m and c is nonzero. If Eq. (15) is reformulated as

$$y = m(x - \bar{x}) + b \quad (16)$$

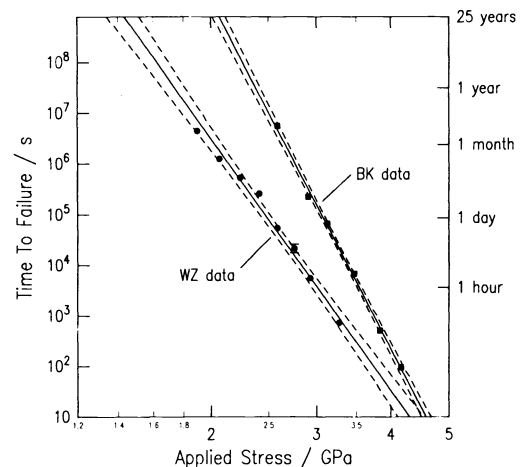


Fig. 1. Power law (model 1) fits to the static fatigue data of Wang and Zupko (1968) (WZ data) and Brownlow and Krause (1991) (BK data).

m and b are uncorrelated so that the variance in the extrapolated value of y , Δy^2 , is related to the variances in m and b , Δm^2 and Δb^2 , by

$$\Delta y^2 = \Delta m^2(x - \bar{x})^2 + \Delta b^2 \quad (17)$$

The confidence intervals in Fig. 1 are determined by calculating the curves for $y \pm 2\Delta y$ and, therefore, represent a 95% confidence interval on the extrapolation. The intersection of the lines with the 25-year axis then gives the maximum allowed stress and its confidence interval for surviving that time. The allowed stress is found to be 1.43 ± 0.09 GPa and 2.07 ± 0.06 GPa for the Wang and Zupko (WZ) and Brownlow and Krause (BK) data, respectively. Therefore, extrapolation of these data using the power law yields estimates with quite modest confidence intervals.

Figure 2 shows the results of fitting all four models under consideration to the WZ data. Models 2 and 4 gave similar predictions of a significantly lower allowed stress than model 1 (the power law) while model 3 predicts an even lower stress. The lack of overlap of the confidence intervals at 25 years shows that for these particular data, uncertainty in the applicable model dominates the statistical uncertainty. Further, the power law gives overly optimistic predictions of allowed stress, considering the lack of evidence to support this model instead of the other models considered.

Figure 3 shows the fits of the four models to the BK data. Here again models 2 and 4 give very similar predictions, but while there is no overlap of the confidence intervals at 25 years, the predicted allowed stress is similar for both model 1 and models 2 and 4. Model 3 predicts a much lower allowed stress, but the very large confidence interval nearly overlaps those for models 2 and 4. For these data, model uncertainty is of a similar magnitude to the statistical uncertainty and cannot be ignored.

The regression fits found that the power law (model 1) gives the best description of the BK data, while model 2 best describes the WZ data (where best description is determined by the highest correlation coefficient and smallest extrapolated confidence bands). Therefore, no one model best fits all data and one is cautioned against choosing one model over the others because it happens to give the best fit.

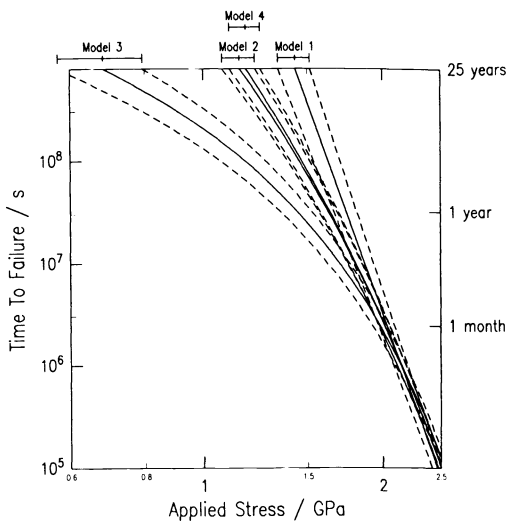


Fig. 2. Extrapolations of the best fits to the WZ data for the four models.

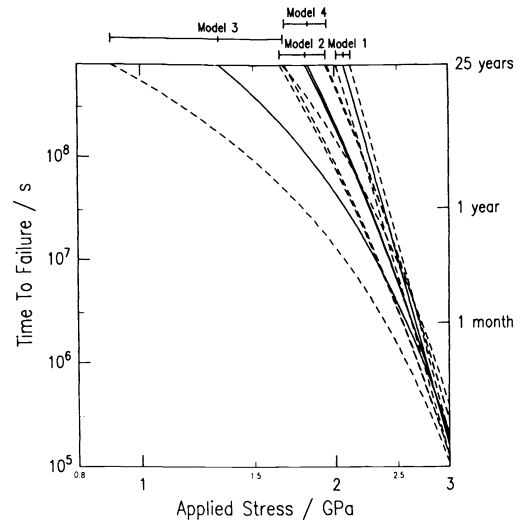


Fig. 3. Extrapolations of the best fits to the BK data for the four models.

The trends in Figs. 2 and 3 are general and are not data specific. For example, models 2 and 4 are always similar, and this can be understood by inspection of Eqs. (11a) and (13). The only difference in form is the appearance in the left-hand side of the equations of σ for model 2 and σ^2 for model 4. Since the range of σ is much smaller than the range of t_f , this difference is negligible. Further, the allowed stress increases in order for predictions of models 3, 2, 4, and 1. This may be proven by constraining the different models to give the same position and gradient on the fatigue curve at some representative applied stress. If this representative stress σ_0 , gives a time to failure t_0 , then we constrain the models to have the same t_f and $dt_f/d\sigma$ at $\sigma = \sigma_0$. This also constrains the fatigue curves for the different models to have the same position and slope at σ_0 for the log-log fatigue plot, such as in Figs. 2 and 3. A sensible position for the constrained point is the median of the fatigue data used for extrapolations. If the inert strength S for the accelerated fatigue data is defined as S_0 , then it may be shown that

$$\frac{n_2}{S_0} \approx \frac{n_1 - 1}{\sigma_0} \quad (18)$$

$$\frac{n_3}{S_0^2} = \frac{n_1 - 2}{2\sigma_0^2} \quad (19)$$

$$\frac{n_4}{S_0} = \frac{n_1 - 2}{\sigma_0} \quad (20)$$

Table 1 compares the fitted values of n_2 , n_3 , and n_4 with the values estimated from Eqs. (18) to (20). In all cases the estimates lie within one standard error of the fitted value. This shows that one may simply estimate the fit parameters for models 2, 3, and 4 from the best fit parameters for model 1. This considerably

Table 1. Comparison of fitted and predicted n values. Errors are one standard deviation. Predicted values are for $\sigma_0 = 2.64$ GPa for WZ data and 3.3 GPa for BK data.

parameter	WZ data		BK data	
	fitted	predicted	fitted	predicted
n_1	16.5 ± 0.8		22.8 ± 0.6	
n_2/S_0	6.00 ± 0.16	5.89	6.53 ± 0.32	6.61
n_3/S_0^2	1.06 ± 0.03	1.04	0.92 ± 0.07	0.95
n_4/S_0	5.64 ± 0.16	5.51	6.25 ± 0.31	6.30

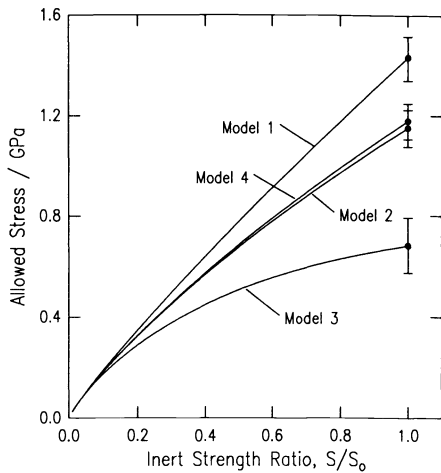


Fig. 4. Maximum allowed stress predictions as a function of the relative inert strength for the WZ data.

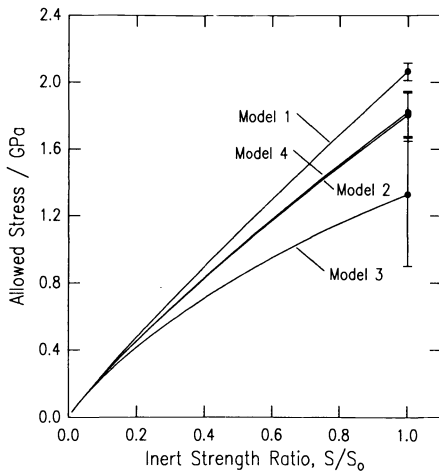


Fig. 5. Maximum allowed stress predictions as a function of the relative inert strength for the BK data.

reduces the work load associated with examining these other models. However, this technique does not provide a means for estimating the uncertainty in the best fit parameters for the other models and should be used with caution.

Equations (10) through (13) have been used to calculate, for each model, the allowed stress for a 25-year design life if the inert strength of the fiber, S , is weaker than the inert strength of the fiber used for accelerated testing, S_0 . The results for both the WZ and BK data are shown in Figs. 4 and 5. The allowed stress is plotted as a function of the inert strength ratio S/S_0 , and, as expected, the allowed stress is lower as the inert strength ratio is reduced from unity. Interestingly, the four models converge for very weak fibers. This may be understood by inspection of Eqs. (6) through (9) where the ratio σ/S may be recognized as the ratio of initial stress intensity to critical stress intensity, which depends on $t_f \sigma^2$ according to these relationships. As $t_f \sigma^2$ approaches $t_0 \sigma_0^2$ (i.e., the data region), stress intensity approaches that in the test data and the extrapolation in stress intensity (which is the source of model differences) tends to zero. The error bars on the 25-year stresses in Figs. 4 and 5 are deduced from Figs. 2 and 3. Confidence intervals on the allowed stresses in Figs. 4 and 5 would decrease as the S/S_0 ratio decreases, implying that the allowed stress would be better determined for weaker fibers. Such confidence intervals have been

deliberately omitted since, as discussed earlier, the fatigue behavior as a function of inert strength is simply not known and, therefore, any extrapolations on inert strength must be considered "best guess."

Since most analysis of fiber fatigue is performed with the power law, a data-independent conversion of these predictions to those that would be obtained by the other models is desirable. Equations (18) to (20) relate the n parameters in a data-independent way. It is readily shown, also, that the A parameters are related by the constraint that all models predict a t_0 lifetime at σ_0 stress. Using these relationships and equating time to failure at the service stress yields the following transcendental equations that relate allowed stress in models 2, 3, and 4 to the prediction of allowed stress from the power law (model 1):

$$\Phi \left(\frac{\sigma_2}{\sigma_1} \right)^2 n_1 \exp(-v) \approx \left[v \Phi^{-r} \left(\frac{\sigma_2}{\sigma_1} \right) + 1 \right] \exp \left[-v \Phi^{-r} \left(\frac{\sigma_2}{\sigma_1} \right) \right], \quad (21)$$

$$\Phi \left(\frac{\sigma_3}{\sigma_1} \right)^2 \exp \left(\frac{-1}{2r} \right) = \exp \left[\left(\frac{-1}{2r} \right) \Phi^{-2r} \left(\frac{\sigma_3}{\sigma_1} \right)^2 \right], \quad (22)$$

$$\Phi \left(\frac{\sigma_4}{\sigma_1} \right)^2 \exp \left(\frac{-1}{r} \right) = \exp \left[\left(\frac{-1}{r} \right) \Phi^{-r} \left(\frac{\sigma_4}{\sigma_1} \right) \right], \quad (23)$$

where

$$\Phi = \left(\frac{t}{t_0} \right) \left(\frac{\sigma_1}{\sigma_0} \right)^2, \quad r = \frac{1}{n_1 - 2}, \quad v = n_1 - 1, \quad (24)$$

where σ_1 , σ_2 , σ_3 , and σ_4 are the predictions of models 1 through 4, respectively, of the allowed stress for lifetime t . The terms σ_0 and t_0 are the stress and time values at the midpoint of the fatigue data where the models are matched in position and slope (characterized in these equations by the power law slope n_1). This formulation makes no assumption about the value of stress, strength, or time, so it is applicable to extrapolations in all of these parameters. Equations (21) to (23) have been solved, with a numerical root finding algorithm, for σ_2/σ_1 , σ_3/σ_1 , and σ_4/σ_1 , respectively, at various Φ and n_1 values. The results are plotted in Fig. 6 for the commonly occurring $n_1 = 20$. Tables 2 through 4 provide results for a broad range of Φ and n_1 values. Figure 6 shows that the divergence between models increases as time to failure is extrapolated farther away from the fatigue data. However, as revealed also by the data-specific Figs. 4 and 5, the differences in time-extrapolated predictions decrease as the strength decreases from that used in the fatigue test. These two effects are modeled by the parameter $\Phi = (t/t_0) (\sigma_1/\sigma_0)^2$, which fully characterizes the degree of difference between models per Eqs. (21) to (24). Tables 2 to 4 show numerically the effects of Φ and n_1 on the differences between models. Model differences are most significant for lower n values. For model 3 especially, quite significant differences from model 1 are revealed. At high

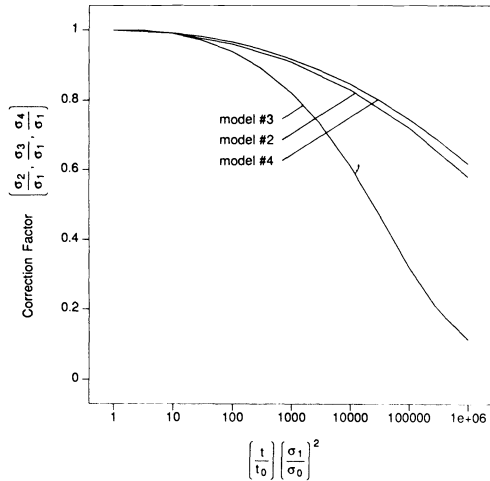


Fig. 6. Conversion of model 1 predictions of allowed stress to models 2, 3, and 4 predictions for $n_1 = 20$.

n values, which are typical of hermetic fiber, Tables 2 to 4 show no significant difference exists between model predictions.

The use of Tables 2 to 4 to translate power law predictions to those of other models is illustrated by the following example: If the available fatigue data has an $n_1 = 20$ slope, a midpoint of $\sigma_0 = 3$ GPa at 1 h, and a power law prediction of $\sigma_1 = 1.62$ GPa acceptable stress for 25 years, then $\Phi = (t/t_0)(\sigma_1/\sigma_0)^2 = 63900$. From Tables 2 to 4, $\sigma_2/\sigma_1 \approx 0.74$, $\sigma_3/\sigma_1 \approx 0.38$, and $\sigma_4/\sigma_1 \approx 0.77$. Thus, the model 2 and 4 predictions are about 1.2 GPa and the model 3 prediction is about 0.6 GPa, in contrast to the power law prediction of 1.62 GPa. The preceding example of high-strength fiber fatigue prediction shows significant differences between models. If the same fatigue data were used to predict fatigue for lower strength fiber, the differences between models would be smaller. For example, if $\sigma_1 = 0.3$ GPa, then $\Phi = 2190$, $\sigma_2/\sigma_1 \approx 0.88$, $\sigma_3/\sigma_1 \approx 0.75$, and $\sigma_4/\sigma_1 \approx 0.90$. These model differences are not negligible, but they are similar in magnitude to the safety margins in many systems.

4. DISPERSION IN FAILURE TIME

A population of similar fibers under nominally similar stress will typically have a significant variation in their static fatigue time to failure. This is explained by the strong dependence of failure time on both stress and strength. Variation in the local environment at different fibers, and other factors, may also contribute to failure time variation. In reliability engineering, predicting the failure time dispersion, or a bound on this quantity, is often desirable. Introducing specific distribution functions for stress and strength into the time-to-failure models [Eqs. (6) to (9)] is possible. However, the resulting expressions for the time-to-failure distribution are unwieldy and not conducive to physical interpretation. A simpler characterization of the relationship between time-to-failure dispersion and stress-and-strength dispersion is obtained by evaluating the derivative of failure time with respect to stress and strength. When these derivatives are evaluated and normalized with respect to the fatigue data midpoint (σ_0, t_0) the following expressions result:

$$\frac{d(\ln t)}{d(\ln \sigma)} = -n_1, \quad \text{model 1} \quad (25)$$

Table 2. Values of σ_2/σ_1 computed from Eq. (21) for various Φ and n_1 values.

Φ	n_1						
	15	20	25	30	40	80	200
1	1.00	1.00	1.00	1.00	1.00	1.00	1.00
10	0.98	0.99	1.00	1.00	1.00	1.00	1.00
100	0.93	0.96	0.98	0.99	0.99	1.00	1.00
10^3	0.83	0.91	0.95	0.97	0.98	1.00	1.00
10^4	0.67	0.83	0.90	0.94	0.97	0.99	1.00
10^5	0.46	0.72	0.84	0.90	0.95	0.99	1.00
10^6	0.36	0.58	0.75	0.84	0.92	0.98	1.00
10^7	0.09	0.40	0.65	0.77	0.89	0.98	1.00
10^8	0.03	0.21	0.55	0.69	0.84	0.97	1.00

Table 3. Values of σ_3/σ_1 computed from Eq. (22) for various Φ and n_1 values.

Φ	n_1						
	15	20	25	30	40	80	200
1	1.00	1.00	1.00	1.00	1.00	1.00	1.00
10	0.98	0.99	0.99	1.00	1.00	1.00	1.00
100	0.88	0.94	0.96	0.98	0.99	1.00	1.00
10^3	0.64	0.82	0.90	0.93	0.97	0.99	1.00
10^4	0.31	0.61	0.78	0.86	0.93	0.99	1.00
10^5	0.10	0.32	0.59	0.75	0.88	0.98	1.00
10^6	0.03	0.11	0.33	0.58	0.81	0.96	1.00
10^7	0.01	0.04	0.12	0.34	0.70	0.95	0.99
10^8	0.003	0.01	0.04	0.14	0.55	0.93	0.99

Table 4. Values of σ_4/σ_1 computed from Eq. (23) for various Φ and n_1 values.

Φ	n_1						
	15	20	25	30	40	80	200
1	1.00	1.00	1.00	1.00	1.00	1.00	1.00
10	0.98	0.99	1.00	1.00	1.00	1.00	1.00
100	0.94	0.97	0.98	0.99	0.99	1.00	1.00
10^3	0.84	0.92	0.95	0.97	0.98	1.00	1.00
10^4	0.70	0.85	0.91	0.94	0.97	0.99	1.00
10^5	0.52	0.75	0.85	0.90	0.95	0.99	1.00
10^6	0.32	0.62	0.77	0.85	0.92	0.98	1.00
10^7	0.16	0.46	0.67	0.79	0.89	0.98	1.00
10^8	0.06	0.30	0.56	0.71	0.85	0.97	1.00

$$\frac{d(\ln t)}{d(\ln S)} = (n_1 - 2), \quad \text{model 1} \quad (26)$$

$$\frac{d(\ln t)}{d(\ln \sigma)} \approx -n_1 - \ln\left(\frac{t_0 \sigma_0^2}{t \sigma^2}\right), \quad \text{model 2} \quad (27)$$

$$\frac{d(\ln t)}{d(\ln S)} \approx (n_1 - 2) + \ln\left(\frac{t_0 \sigma_0^2}{t \sigma^2}\right), \quad \text{model 2} \quad (28)$$

$$\frac{d(\ln t)}{d(\ln \sigma)} = -n_1 - 2 \ln\left(\frac{t_0 \sigma_0^2}{t \sigma^2}\right), \quad \text{model 3} \quad (29)$$

$$\frac{d(\ln t)}{d(\ln S)} = (n_1 - 2) + 2 \ln\left(\frac{t_0 \sigma_0^2}{t \sigma^2}\right), \quad \text{model 3} \quad (30)$$

$$\frac{d(\ln t)}{d(\ln \sigma)} = -n_1 - \ln\left(\frac{t_0 \sigma_0^2}{t \sigma^2}\right), \quad \text{model 4} \quad (31)$$

$$\frac{d(\ln t)}{d(\ln S)} = (n_1 - 2) + \ln\left(\frac{t_0 \sigma_0^2}{t \sigma^2}\right). \quad \text{model 4} \quad (32)$$

Since the $t \sigma^2$ values of interest for reliability prediction are greater than $t_0 \sigma_0^2$, $\ln(t_0 \sigma_0^2 / t \sigma^2) < 0$. Equations (25) to (32), there-

fore, show that the power law (model 1) predicts a broader time-to-failure distribution than models 2 to 4. Depending on the type of reliability analysis, a broad time-to-failure distribution may be conservative or nonconservative. If lognormal distributions for stress and strength are used, then Eqs. (25) through (32) allow a direct estimate of the variance in the log of failure time. This is a linearized approximation (since only the first derivatives of time are considered), which is most valid for small variations in stress or strength. When both stress and strength are distributed, time-to-failure dispersion can be computed as the sum of the variance contributions for stress and strength (assuming these are uncorrelated).

Equations (25), (27), (29), and (31) also model the $d(\ln t)/d(\ln \sigma)$ slope changes with time seen graphically in Figs. 2 and 3. Furthermore, these equations show that the $d(\ln t)/d(\ln \sigma)$ slope becomes more strongly negative as the strength decreases (i.e., σ decreases with respect to σ_0). Bouten mentions this trend for model 2 (Ref. 26) and proposes that this model (in contrast to model 1) is consistent with the observation that n values in bulk glass (large flaws, low test stress) are greater than those for fiber (small flaws, large test stress). Equations (25), (27), (29), and (31) allow quantification of the slope change for models 1 to 4. Use of these relationships with appropriate data may help to identify the most accurate fatigue model.

5. PROOF TESTING

Fiber may be significantly weaker than the typical 5 to 6 GPa short length in-air strength either because (1) the fiber is long in length and affected by the occasional draw line flaws or (2) the fiber is subject to handling or other processing (like fiber splicing) that can weaken it. In these cases, the lowest possible strength may be unacceptable so a proof test is commonly used to eliminate the weakest flaws. Two approaches to modeling the reliability of proof-tested fiber are (1) minimum lifetime²⁷ and (2) interpretation of the proof test as a short-term fatigue test.²⁸ In approach 1, the minimum inert strength after proof testing is assumed to be equal to the proof test stress. The advantage of this method is conceptual simplicity, but the disadvantages are a need for inert strength measurement and the neglect of fiber weakening during proof test unload. Approach 2 treats the proof test as a fatigue test of sorts and formulates the problem in a probabilistic sense with model 1 assumed. The result is a formulation that considers weakening during proof test unload and does not require an inert strength measurement.

No matter which proof test modeling technique is used, power law predictions of allowed stress on proof-tested fiber can be translated to model 2, 3, or 4 predictions via Eqs. (21) to (24) or Tables 2 to 4. To do so, however, does entail the new assumption that the power law prediction of fiber weakening from proof testing is consistent with predictions from other models. The validity of this assumption is addressed by the following analysis. Weakening of a fiber under a constant stress may be characterized by integrating Eqs. (1) through (4) and introducing Eq. (5) to give the following expressions:

$$t = \frac{2K_{IC}^2}{A_1 Y^2 (n_1 - 2)} \sigma^{-n_1} (S_i^{n_1-2} - S_f^{n_1-2}), \quad (33)$$

$$= \frac{2K_{IC}^2}{A_2 n_2^2 Y^2} \sigma^{-2} \left[\left(\frac{n_2 \sigma}{S_i} + 1 \right) \exp\left(\frac{-n_2 \sigma}{S_i} \right) \right.$$

$$\left. - \left(\frac{n_2 \sigma}{S_f} + 1 \right) \exp\left(\frac{-n_2 \sigma}{S_f} \right) \right], \quad (34)$$

$$= \frac{K_{IC}^2}{A_3 n_3 Y^2} \sigma^{-2} \left\{ \exp\left[-n_3 \left(\frac{\sigma}{S_i} \right)^2 \right] \right.$$

$$\left. - \exp\left[-n_3 \left(\frac{\sigma}{S_f} \right)^2 \right] \right\}, \quad (35)$$

$$= \frac{2K_{IC}^2}{A_4 n_4 Y^2} \sigma^{-2} \left[\exp\left(\frac{-n_4 \sigma}{S_i} \right) - \exp\left(\frac{-n_4 \sigma}{S_f} \right) \right], \quad (36)$$

for models 1 through 4, respectively, where S_i is the initial inert strength and S_f is the final inert strength. [Equations (33) through (36) reduce to Eqs. (6) through (9) for time to fracture, when S_f is significantly less than $S_i = S$.] If we assume, conservatively, that the unload portion of the proof test is slow, then no minimum inert strength exists after proof testing. The degree of weakening introduced by proof testing can then be characterized by normalizing the initial inert strength S_i to the maximum initial inert strength that breaks during the proof test, S_{ib} . For each model, S_{ib} is determined from the corresponding expression from Eqs. (33) through (36) using $\sigma = \sigma_p$, the proof test stress, $t =$ the proof test time (or effective proof test time to account for loading and unloading stages), $S_{if} = 0$ (i.e., fiber breaks at the very end of the proof test), and $S_i = S_{ib}$. Introducing the resulting expressions along with Eqs. (18) through (20) into Eqs. (33) through (36) gives the following expressions that relate the degree of fiber weakening S_f/S_i to the normalized initial inert strength S_i/S_{ib} :

$$\left(\frac{S_f}{S_i} \right) = \left[1 - \left(\frac{S_i}{S_{ib}} \right)^{-1/r} \right]^r, \quad \text{model 1} \quad (37)$$

$$\left(v \frac{S_i}{S_{ib}} + \frac{1}{R} \right) \exp[-vR(S_i/S_{ib})] \approx \left(v + \frac{1}{R} \right) \exp(-vR)$$

$$- \left(v \frac{S_i}{S_f} + \frac{1}{R} \right) \exp[-vR(S_i/S_f)], \quad \text{model 2} \quad (38)$$

$$\left(\frac{S_f}{S_i} \right)^{-2} = \frac{-2r}{R^2} \ln \{ \exp[-(R^2/2r)]$$

$$- \exp[-(R^2/2r)(S_i/S_{ib})^2] \}, \quad \text{model 3} \quad (39)$$

$$\left(\frac{S_f}{S_i} \right)^{-1} = \frac{-r}{R} \ln \{ \exp[-(R/r)]$$

$$- \exp[-(R/r)(S_i/S_{ib})] \}, \quad \text{model 4} \quad (40)$$

where

$$R = \left(\frac{\sigma_p}{\sigma_0} \right) \left(\frac{S_0}{S_i} \right), \quad r = \frac{1}{n_1 - 2}, \quad v = n_1 - 1. \quad (41)$$

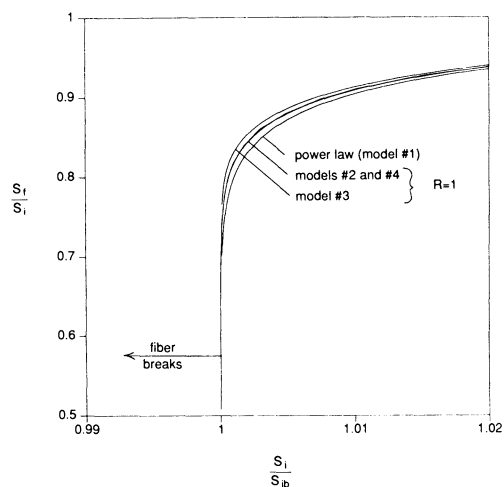


Fig. 7. Comparison of proof test weakening predictions for models 1 through 4.

The nondimensional parameter R is typically greater than 1.0. (It can be shown that $R \geq 1$ if $t\sigma^2$ for the proof test is less than $t_0\sigma_0^2$). Except for Eq. (38), these expressions are solved readily in closed form. A numerical solution to Eq. (38) was obtained with a root-finding algorithm. The results for all models [Eqs. (37) through (40)] are plotted in Fig. 7 for $R = 1$ and $n_1 = 20$. This figure shows the power law model to be the most pessimistic in terms of predicting fiber weakening during proof test for the conservative case of slow unloading. It is readily shown that this conclusion is independent of n_1 and R for $R > 1$. Therefore, when a power law prediction of allowed stress on proof-tested fiber (where slow unloading is assumed) is converted to a different model prediction via Eqs. (21) through (24), the results will be somewhat conservative because the most pessimistic model of strength truncation will be assumed.

6. SUMMARY AND DISCUSSION

Analysis in this paper has shown that the uncertainty in the crack growth model cannot be ignored in making reliability predictions for optical fiber under stress. The statistical uncertainty is significant also, but is usually smaller than the model uncertainty. The differences in allowed stress predictions between models become quite large at long times, especially for fiber of the same strength as that used in the fatigue test. Clearly, it would be desirable to know which model most accurately characterizes the fatigue process. Unfortunately, the current understanding of crack growth does not allow us to determine the most accurate model, so engineering judgment is required to determine the appropriate degree of conservatism for a given application. However, it seems clear that the power law model is not appropriate given its lack of a physical basis and its optimism compared with other models that also fit the available fatigue data well.

A common application of fiber fatigue models is to predict allowed stress on fiber that is significantly weaker than the fatigue-tested fiber. Analysis in this paper has shown that for such cases, the differences in model predictions become small. This fact and the common use of design safety factors may explain the generally positive field reliability of optical fiber systems designed with power law analysis. However, since model differences are quite large for some applications, universal use of the power law model is not recommended.

While models 2 to 4 (the nonpower law models) are mathematically "messier," this paper shows that static fatigue analysis with these models is tractable. Since model 4 yields significantly simpler forms but similar predictions to model 2, perhaps this latter model is not needed. On the other hand, model 2 seems to have the strongest physical basis of any of the models.

The development of data-independent conversions of allowed stress prediction from the power law to other models provides a quick way to assess the difference between models. It has been shown that when this correction is applied to predictions for proof tested fiber, some conservatism is introduced. Relationships between time-to-failure dispersion and strength-and-stress dispersion are important to many reliability analyses, and may also aid in the physical interpretation of fatigue data. It is shown that a linearization of this relationship leads to simple expressions that allow failure time dispersion estimates for each of the models. We hope that further work in optical fiber fatigue will yield a greater understanding of the crack growth process so that model uncertainty is reduced and the reliability prediction job becomes more straightforward and less risky.

7. ACKNOWLEDGMENTS

The authors thank Daryl Brownlow, Harish Chandan, and John Krause for static fatigue data. One of us [MJM] acknowledges useful discussions on activation energy with Chuck Kurkjian.

8. REFERENCES

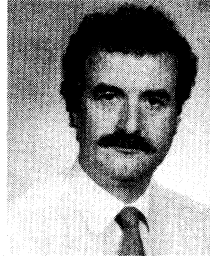
1. J. E. Ritter, Jr., N. Bandyopadhyay, and K. Jakus, "Statistical reproducibility of the dynamic and static fatigue experiments," *Ceramic Bul.* 60, 798-806 (1981).
2. G. M. Bubel, J. T. Krause, B. J. Bickta, and R. T. Ku, "Mechanical reliability of metallized optical fiber for hermetic terminations," *J. Lightwave Tech.* 7, 1488-1493 (1989).
3. K. Jakus, J. E. Ritter, and J. M. Sullivan, "Dependency of fatigue predictions on the form of the crack velocity equation," *J. Amer. Ceram. Soc.* 64, 372-374 (1981).
4. R. H. Doremus, "Fatigue in glass," in *Strength of Inorganic Glass*, C. R. Kurkjian, ed., Plenum, New York, 231-248 (1985).
5. G. G. Trantina, "Strength and life prediction for hot-pressed silicon nitride," *J. Amer. Ceram. Soc.* 62, 377-380 (1979).
6. S. M. Wiederhorn, "A chemical interpretation of static fatigue," *J. Amer. Ceram. Soc.* 55, 81-85 (1972).
7. T. A. Michalske and B. C. Bunker, "Slow fracture model based on strained silicate structures," *J. Appl. Phys.* 56, 2286-2693 (1984).
8. T. A. Michalske and B. C. Bunker, "Steric effects in stress corrosion fracture of glass," *J. Amer. Ceram. Soc.* 70, 780-784 (1987).
9. H. H. Yuce, A. D. Hasse, and P. L. Key, "Effect of common chemicals on the mechanical properties of optical fibers," *Proc. SPIE* 992, 211-219.
10. J. T. Krause, "Zero stress strength reduction and transitions in static fatigue of fused silica fiber lightguides," *J. Non-Cryst. Solids* 38 and 39, 497-502 (1980).
11. M. J. Matthewson and C. R. Kurkjian, "Environmental effects on the static fatigue of silica optical fiber," *J. Amer. Ceram. Soc.* 71, 177-183 (1988).
12. C. R. Kurkjian and U. C. Paek, "Single-valued strength of 'perfect' silica fibers," *Appl. Phys. Lett.* 42, 251-253 (1983).
13. D. Roberts, E. Cuellar, L. Middleman, and J. Zucker, "Static fatigue of optical fibers in bending," presented at SPIE '86, Cambridge, MA, September 25-26, 1986.
14. J. T. Krause and C. J. Shute, "Temperature dependence of the transition in static fatigue of fused silica optical fiber," *Adv. Ceram. Mat.* 3, 118-121 (1988).
15. H. H. Yuce, A. J. Colucci, P. L. Key, and M. A. Andrejco, "Strength and fatigue behavior of low strength optical fibers," *Proc. OFC* 89, paper WA2 (1989).
16. T. P. Dabbs and B. R. Lawn, "Strength and fatigue properties of optical glass fibers containing microindentation flaws," *J. Amer. Ceram. Soc.* 68, 563-569 (1985).
17. B. L. Lin, M. J. Matthewson, and G. J. Nelson, "Indentation experiments on silica optical fibers," in *Fiber Optic Reliability: Benign and Adverse Environments*, *Proc. SPIE* 1366, 157-166 (1990).
18. R. J. Charles, "Static fatigue of glass. II," *J. Appl. Phys.* 29, 1554-1560 (1958).
19. A. G. Evans, "Slow crack growth in brittle materials under dynamic loading conditions," *Int. J. Fracture* 10, 251-259 (1974).

20. W. S. Hillig and R. J. Charles, in *High Strength Materials*, V. F. Zackay, ed., Wiley, New York, pp. 682-705 (1965).
21. B. R. Lawn, "An atomistic model of kinetic crack growth in brittle solids," *J. Mat. Sci.* 10, 469-480 (1975).
22. E. M. Lenoe and D. M. Neil, "Assessment of strength-probability-time relationship in ceramics," AMMRC Tech. Rept. No. 75-13, ARPA Order No. 2181 (June 1975).
23. C. K. Kao, "Optical fibre and cables" in *Optical Fiber Communications*, M. J. Howes and D. V. Morgan, eds., pp. 189-250, Wiley, New York (1980).
24. T. T. Wang and H. M. Zupko, "Long-term mechanical behavior of optical fibers coated with a UV-curable epoxy acrylate," *J. Mat. Sci.* 13, 2241-2248 (1978).
25. D. L. Brownlow, H. C. Chandan, and J. T. Krause, Private communications (1991).
26. P. C. P. Bouten, "Lifetime of pristine optical fibers," Ph.D. thesis, University of Eindhoven (1987).
27. A. G. Evans and S. M. Weiderhorn, "Proof testing of ceramic materials—an analytic basis for failure prediction," *Int. J. Fracture* 10, 379-392 (1974).
28. Y. Mitsunaga et al., "Failure prediction for long length optical fiber based on proof testing," *J. Appl. Phys.* 7, 4847-4853 (1982).



Gregory M. Bubel graduated with honors and with highest distinction from the Pennsylvania State University in 1983 with the BS degree in mechanical engineering. As a National Science Foundation fellow, he researched vibration modeling at Purdue's Herrick Laboratories and received the MS degree in mechanical engineering from Purdue University in 1985. In 1985 he joined AT&T Bell Laboratories where he has investigated the reliability of mechanical, electrical, and optical

components for undersea fiber optic communications systems, with emphasis on the mechanical properties and fatigue of optical fibers.



M. John Matthewson received his BA in theoretical physics in 1975 from Cambridge University, where he was a Kitchener Scholar and a Prize Scholar. He obtained MA and Ph.D. degrees in 1978, also from Cambridge University, for his work at the Cavendish Laboratory on contact mechanics and high-speed fracture. He then continued his research in this area as concurrently the Goldsmiths Junior Research Fellow at Churchill College, Cambridge, and as a Science Research Council Postdoctoral Fellow. After three years as a consultant in the Cambridge University Computing Service, in 1984 he moved to AT&T Bell Laboratories as a postdoctoral member of the technical staff, where he worked on optical fiber strength and fatigue. From 1986 to 1989, he was an advisory engineer at IBM Almaden Research Center, San Jose, where he worked on reliability of magnetic recording devices and various aspects of adhesion. He is now an associate professor in the Fiber Optic Materials Research Program at Rutgers University, where his research group is concerned with strength and fatigue of optical materials in general and oxide and nonoxide fibers in particular.